Biomimetic assembly of polyelectrolyte multilayers containing phosvitin monitored with reflectometric interference spectroscopy

Steffi Grohmann, Holger Rothe, Susanne Eisenhuth, Christian Hoffmann, and Klaus Liefeith[a)]
Department of Biomaterials, Institute for Bioprocessing and Analytical Measurement Techniques (IBA), Rosenhof, 37308 Heilbad Heiligenstadt, Germany

(Received 21 March 2011; accepted 19 April 2011; published 16 May 2011)

Coatings of biomaterials or implants that facilitate biomineralization possess a great potential for applications focused to the replacement, augmentation, and regeneration of bone tissue. Biomimetic approaches utilize biomolecules for either templating or supporting the crystallization process. One of these promising biomolecules is phosvitin (PV), an egg yolk protein known to transport and store inorganic phosphates and calcium ions. The incorporation of PV into polyelectrolyte multilayers is favorable due to PVs high degree of phosphorylation and thus a high acidity. Utilizing the reflectometric interference spectroscopy, the adsorption kinetics of this novel polyelectrolyte system composed of poly-L-lysine and the heavily phosphorylated phosvitin were monitored. The results demonstrate an unexpected nonregular growth regime called overshoot. Effective measures of shifting this irregular polyelectrolyte adsorption process back to a regular multilayer growth regime are reported in this paper. © *2011 American Vacuum Society.* [DOI: 10.1116/1.3589176]

I. INTRODUCTION

Since their introduction in the 1990s, polyelectrolyte multilayer (PEM) coatings deposited by the "layer by layer" technique received ever growing attention.[1] Especially in the field of life sciences, a multitude of applications based on PEM coating arose throughout the last decade (reviewed in Refs. 2–4). Former attempts of generating mineralized extracellular matrix-like coatings on biomaterial surfaces in contact with bone have shown a high potential of PEM films to serve as an organic matrix for the incorporation of calcium phosphates.[5,6] In order to biomimetically calcify PEM coatings, a calcification technology based on templating molecules is desirable and, thus, a careful choice of PE is of pivotal importance. The egg yolk protein phosvitin (PV) may be a promising biomolecule to be incorporated within PEM films since it was described to facilitate biological calcification processes *in vivo*.[7] Phosvitin is a subdomain of the egg yolk protein vitellogenin. Upon endocytosis in the oocyte, vitellogenin is proteolytically processed by the endosomal protease cathepsin D (reviewed in Ref. 7) to yield lipoproteins and phosphoproteins such as PV. According to Milhofer *et al.*,[8] PV contains up to 47 mol % of serine residues, 98% of which are phosphorylated. PV is, furthermore, described to bind, transport, and store trace metals (such as zinc and copper), but even more interesting also Ca^{2+} and inorganic phosphate (P_i) ions. It is reported to have antioxidant functions (reviewed in Ref. 9) and it supports mineralization in vertebrate embryos.[7] Due to this high proportion of post-translationally phosphorylated serine residues PV displays acidic properties that are well utilizable for an electrostatic PEM construction.[10] However, up to date no data were published for the construction of PEM films with PV. This is the first report of building PEM coatings from the bioactive protein PV.

Though the layer by layer technique is a simple and versatile technology for preparing biomaterial coatings, sometimes the chosen polyelectrolytes do not result in stable film growth. Especially for weak ionic groups such as tertiary amines and carboxylic acids that are typically presented on protein surfaces, instabilities in the build-up process (also called overshoot) are reported.[11,12] These overshoots in PEM assembly often occur in a time frame of a few seconds and are correlated with film erosion. Consequently, a careful online monitoring of PEM film growth with a high temporal resolution is of fundamental importance for generating biomimetic material coatings. Surface analytical measurement techniques employed to monitor PEM film growth comprise the following: optical waveguide light microscopy,[13,14] quartz microbalance[15,16] (QCM-D), ellipsometry,[17,18] surface plasmon resonance (SPR),[19] absorption measurements (vis and near UV),[20] and infrared spectroscopy.[20,21] This is the first study on the analysis of PEM film growth *in situ* using reflectometric interference spectroscopy (RIfS). Due to its high accuracy and resolution, the RIfS technique has primarily been utilized for biomolecular interaction analysis (BIA) up to date.[22] Figure 1 summarizes the basic principles underlying the RIfS detection. The RIfS transducer consists of a glass substrate with a 10 nm Ta_2O_5 interference layer and a 300 nm SiO_2 coating on top (Fig. 1). Briefly, a light beam perpendicularly directed onto the biosensor surface coated with the molecules of interest (not depicted in Fig. 1) is reflected at the two different interfaces, (i) SiO_2 versus Ta_2O_5 (beams 1 and 1′) and (ii) the organic coating versus buffer (beams 2 and 2′). Since the two reflected beams are traveling on different path lengths, with the difference in path length corresponding to two times the layer thickness of the deposited organic material, a phase difference can be

a)Electronic mail: klaus.liefeith@iba-heiligenstadt.de

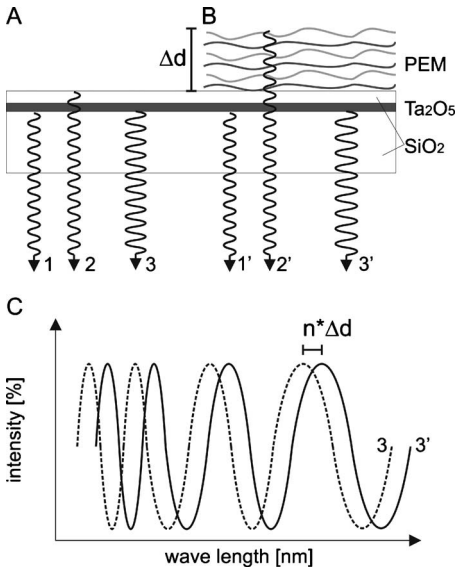

FIG. 1. Schematic representation of the RIfS detection. A light beam perpendicularly directed onto the transducer surface (from the bottom of the transducer, not depicted for clarity) is reflected at the interface between SiO_2 and Ta_2O_5 corresponding to 1 and 1′. An additional reflection occurs at the interface toward the aqueous media (beams 2 and 2′) causing positive and negative interferences with the latter beam. The resulting interference spectrum is depicted in C for 3 and 3′. The phase difference between 3 and 3′ in C corresponds to the difference in optical thickness between A and B [uncoated transducer and transducer coated with three bilayers of polyelectrolytes (PEM), respectively].

observed. This phase difference results in both positive and negative interferences depending on the respective wavelength and is recorded as an interference spectrum (beams 3 and 3′ in Fig. 1). A change in optical thickness of the deposited coating causes a measurable shift in the interference spectrum. In this article, the PEM buildup of different polyelectrolyte systems is examined *in situ* utilizing the RIfS technology. The film construction of the well described model system composed of the polypeptides poly-L-lysine (PLL) and poly-L-glutamic acid (PGA) was investigated by means of atomic force microscopy (AFM) and online ellipsometry in a flow cell in order to validate the results obtained with RIfS.[23] Of particular interest is the analyzed growth kinetic of PLL-PV assemblies. It is of value to point out that these novel bioactive PEM films with the phosphoprotein PV (polyanion) display a high potential for applications in biomaterial research.

II. EXPERIMENT

A. Multilayer film preparation

All chemicals were purchased from Sigma (Germany) in the highest purity available and used without further purification. PLL (P2636, MW 30–70 kD), FITC conjugated poly-L-lysine (PLL-FITC, P3069, MW 30–70 kD), poly-L-glutamic acid (PGA, P4886 MW: 50–100 kD), and phosvitin (PV, P1253) were dissolved in a Hepes/NaCl buffer (25 mM Hepes, 137 mM NaCl, *p*H 7.4) at a concentration of 1 mg/ml and sterile filtered (0.2 μm). As indicated in Sec. III for some experiments the NaCl and polyelectrolyte concentrations were lowered to 50 mM and 0.1 mg/ml, respectively. Films were manually produced by alternately depositing the polycation (PLL) and polyanion (PGA or PV) layers onto the substrate. The incubation time for each polyelectrolyte solution was 5 min followed by three cycles of rinsing with Hepes/NaCl buffer. Borosilicate disks (B33, 4H Jena Engineering, Germany) and silicon wafers were used as substrates for PEM construction. Initially, all surfaces were cleaned with detergents (SDS) and pure water (Millipore) and the surface was preactivated by etching with either 0.1*M* HCl or 35% HNO_3 (v/v).

B. RIfS

RIfS analyses of the PEM film formation and the adsorption of proteins on different PE layers were carried out with the BIAffinity system (Analytik Jena AG, Germany). The PEM films were deposited onto transducer surfaces (Analytik Jena AG, Germany) within a flow cell (dimensions of 6 mm × 1 mm × 125 μm). Blank transducers (from here on are called chips) were preactivated by incubation with 100 μl of 35% HNO_3 for 10 s followed by extensive rinsing with de-ionized water before they were mounted within the system. All buffers and solutions employed for coating in the BIAffinity system were filtered (0.2 μm) and degassed before use. At a buffer flow rate of 10 μl/min, the activated chip was washed until a stable baseline signal was obtained. PEM film deposition was always initiated by injecting 30 μl of PLL (at 10 μl/min) followed by a rinsing time of at least 5 min. All further injections were always carried out with 30 μl of the respective PE or protein at a flow rate of 10 μl/min until the desired film architecture was received. Data were recorded in 1 s intervals and presented as the shift of the spectral interference which corresponds to the optical thickness of the resulting PEM film. AFM measurements were performed in order to validate the film thicknesses obtained by RIfS. Difficulties in locating the respective edges of the deposited coatings were overcome by utilizing an AFM coupled with a fluorescence microscope detection unit (for details, see Sec. II D). Fluorescence labeling was accomplished at a 90° angle (in two flow channels) with respect to the PEM film buildup process resulting in two squares where the two chambers overlap [Fig. 2(a)]. Fluorescently labeled PLL (PLL-FITC) was injected as described above and the stained chips were protected from light until AFM analyses were performed.

C. Ellipsometry

The ellipsometric angles delta (Δ) and psi (Ψ) were recorded with an imaging ellipsometer (EP3, Nanofilm, Göttingen, Germany) equipped with both a 532 nm laser and a full spectrum lamp (Xenon Short ARC®, Osram). PEM film ($n=1.42$, $k=0$) thicknesses on silicon (SiO_2: $n=1.455$, $k=0.00$, $d=3$ nm, Si: $n=4.16$, $k=0.049$) were recorded at wavelengths of 532 and 643 nm with an angle of incidence of 42°. For imaging measurements Δ and Ψ maps of

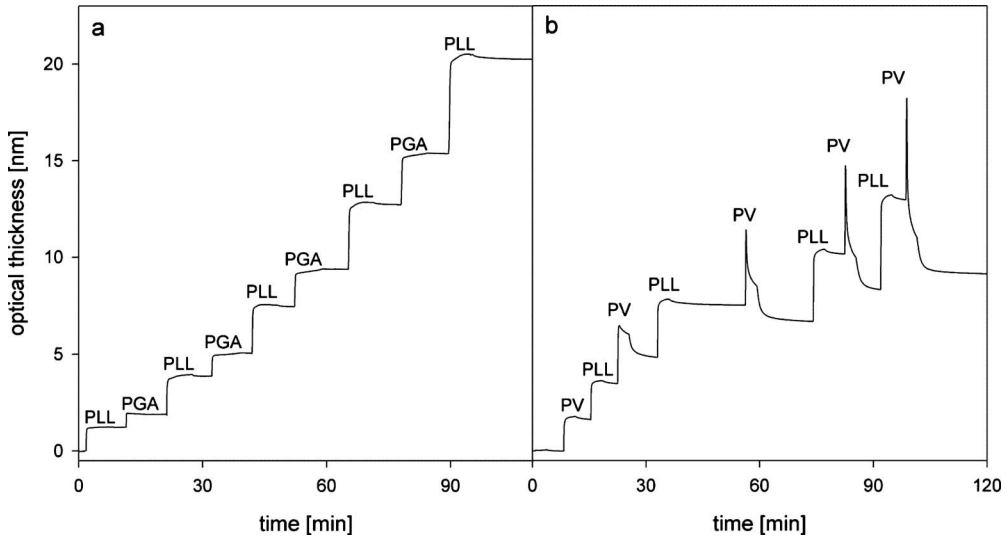

FIG. 2. Analysis of PEM film growth presented as the change in optical thickness (n^*d) over the experimental time monitored with RIfS. PE deposition was performed by alternately injecting PLL and the respective polyanion solutions. (a) Film construction from PLL and PGA displays a regular stepwise increase in film thickness which follows an exponential growth regime. (b) Construction of PEM films from PLL and PV displays a sharp increase in optical thickness followed by a drastic reduction in film thickness after a few seconds solely when injecting PV.

460 μm$\times$460 μm were recorded. The obtained angles were transformed into film thicknesses by employing a fixed n and k model implemented within the software.

Time resolved ellipsometric measurements were carried out using a commercially available flow chamber equipped with optical windows (SL-cell, Nanofilm, Göttingen, Germany) and a rotary lobe pump (Ismatec, Germany). Before assembling the chamber, substrates were cleaned and preactivated as described above and the laser was focused on the substrate surface (λ=532 nm, aoi=60°). All buffers and solutions were treated as described for the RIfS measurements. Coating was carried out by sequentially pumping (0.5 ml/min) the polyelectrolyte into the flow chamber followed by an incubation period without flow of 6 min and finally rinsing the chamber with buffer. This procedure was carried out until the desired number of layers was deposited.

D. AFM

The atomic force microscope (JPK Nanowizard® with a CellHesion® module) is equipped with an inverse microscope (Zeiss, Axio Observer with fluorescence detection) and was used for topographical analysis and force-induced ablation of PEM films generated on different surfaces. All measurements were performed in a special fluidic cell (Smart Cell®, JPK, Germany) rinsed with Hepes/NaCl buffer in contact mode. The employed cantilever (Si_3N_4, tip radius $<$20 nm, spring constant of 52.6 mN/m) was cleaned in a plasma cleaner before use and the analyzed PEM films were allowed to equilibrate 15 min before the measurements. Topography scans of PEM films on wafers were performed with a set point of 0.35 V (approximately 8 nN) and force-induced ablation/scratching was accomplished with 7 V (approximately 150 nN). Fluidic channels on the transducer surfaces were visualized by fluorescence microscopy [excitation: mercury lamp with FITC filter set (450 nm–490 nm); detection: full emission spectrum] after labeling the PEM film with PLL-FITC.

E. Turbidity measurements

The formation and stability of polyelectrolyte complexes (PECs) were investigated in order to evaluate the influence of different salt concentrations (50, 137, and 200 mM NaCl) on the formation of PLL-PV multilayers. Since PECs are insoluble complexes, they cause a turbidity of the solution that can easily be quantified with absorption measurements at 400 nm. Equal volumes of PV and PLL solutions were combined to yield defined ratios of the polycations (PLL) to polyanions (PV) in solution. The mass ratio R^+ of PLL chains in solution was defined as $R^+=V_{PLL}/(V_{PLL}+V_{PV})$ (V_{PLL} and V_{PV}=volume of the PE solutions). The mixtures were prepared from PV and PLL solutions containing 1 or 0.1 mg/ml of the respective polyelectrolyte. After the preparation of samples with varying R^+, the turbidity was recorded at 400 nm. Absorbencies were transformed to relative absorbencies with the maximum absorbance defined as 1 and the minimum absorbance set to 0.

III. RESULTS AND DISCUSSION

To the best of our knowledge, this is the first report of the *in situ* monitoring the PEM construction from PLL and the phosphoprotein phosvitin. Since instabilities in film buildup proceed in a few seconds and can only be detected with online measurements, the RIfS was employed for this study. Due to the fact that RIfS was never utilized for investigations on film growth, we first performed validating characterizations on the well described reference PEM system $(PLL\text{-}PGA)_i$ with RIfS, ellipsometry, and AFM. For $(PLL\text{-}PGA)_i$ assembly a stepwise increase in optical thick-

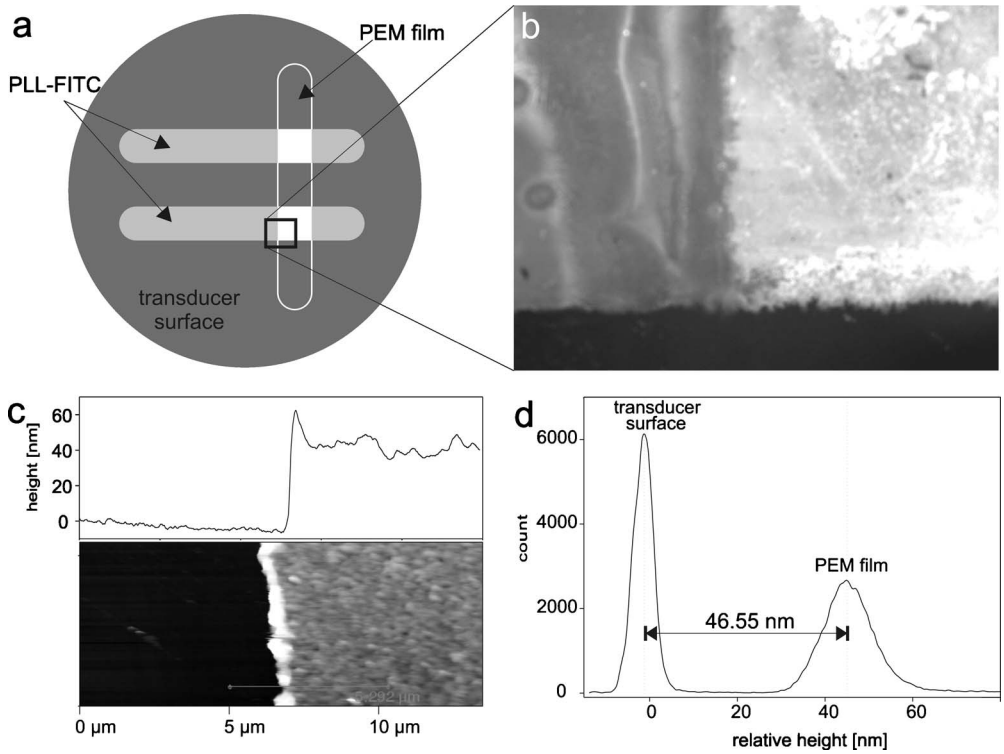

FIG. 3. AFM analyses on structured PEM films: (a) sketch of the coated RIfS transducer surface (dark gray) before AFM analysis. The PEM film constructed (white framed dark gray fluidic channel) is fluorescently labeled with PLL-FITC in a rectangular angle (light gray bars). (b) Fluorescence microscope image at the intersection of four different zones (upper left: only PLL-FITC; upper right: PLL-FITC stained PEM film; lower right: unstained PEM film; lower left: bare transducer surface; image size 900 μm $\times$ 675 μm). (c) Topographical analysis of the film thickness at the coating border with the corresponding height profile. (d) Results of statistical evaluation of height data collected with the AFM.

ness upon the alternating deposition of the oppositely charged polyelectrolytes was detected (Fig. 2). Furthermore, the film growth follows an exponential regime which is described in more detail elsewhere.[18,24,25] To transform the measured optical thickness (n*d) into a film thickness (d), we assumed a refractive index for the PEM film of 1.42 according to data published by Richert *et al.*[26] The resulting data for the $(PLL\text{-}PGA)_i$ film construction are in good accordance with the data reported in the literature in terms of adsorption kinetics and actual layer thickness.[23]

After monitoring the PEM film growth *in situ* [dark gray bar framed in white, Fig. 3(a)] utilizing the RIfS technology, the coated transducers were rotated (90°) and again mounted within the system. Subsequently, FITC labeled PLL [PLL-FITC, light gray bars in Fig. 3(a)] was injected through two fluidic channels in order to stain the PEM film at the intersection of the two channels [white square, Fig. 3(a)]. The fluorescence detection unit mounted onto the AFM facilitates the localization of the PEM coated areas and their edges. Figure 3(b) represents a microscope image of the four zone intersection of the stained PEM films on the transducer surface. In the upper right section of the image, a bright fluorescence signal was detected for the stained PEM film. As expected, no fluorescence was detected for either the unstained PEM film or the unstained transducer surface (lower right and lower left parts, respectively). Although less intensive, fluorescence signals were detected for the transducer surface not precoated with a PEM film but stained with PLL-FITC as well. However, a single monolayer of FITC conjugated PLL does not result in a fluorescence signal as intense as the signal for the multilayered PEM film (upper right zone). PLL-FITC has been demonstrated to diffuse freely over the whole thickness of a PEM film.[27,28] Thus, thicker PEM films can accumulate more PLL-FITC molecules resulting in an increased fluorescence intensity.

From the topography scans, the film thickness can either be estimated from a line scan over the edge of the coated area [Fig. 3(c)] or through statistical analysis of all heights measured in one scanned field as depicted in Fig. 3(d). The thickness determined by AFM measurements is approximately 6 nm lower than the film thickness recorded with RIfS for a nine double layer film construct. This difference in the determined film thickness may be explained by the scanning area of the employed techniques. While the RIfS data are based on an average scanning area of $\sim$1 mm^2, the statistical analyses of the AFM height information were performed using a scanning area of $\sim$100 μm^2 (10,000-fold smaller sample area). Nevertheless, with respect to the standard deviation of the AFM data, the determined PEM thicknesses correlate well with the data obtained from the RIfS analysis. An underestimation of the film thickness caused by a compression of the film by the cantilever tip was proven to

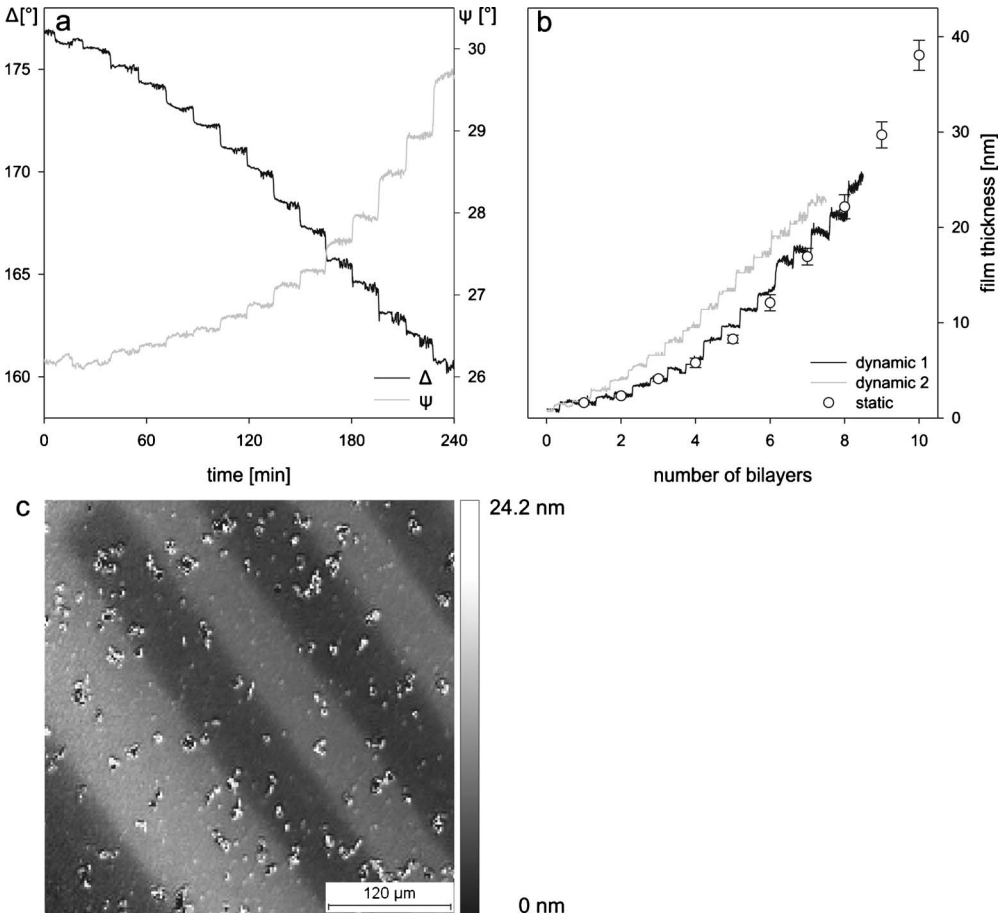

FIG. 4. Time resolved ellipsometric measurements of the $(PLL\text{-}PGA)_i$ film growth. (a) Raw data plotted as Δ and Ψ vs time recorded for the dynamic PEM construction within a fluidic cell. (b) Modeled film thicknesses over the number of bilayers for the dynamic PE deposition (lines) and for ellipsometry on dried PEM films constructed statically (dots). (c) Thickness map obtained from imaging ellipsometry measurements on a PEM film patterned with photoablation.

be in a negligible range. A low set point was chosen, and nearly no differences in the height images obtained from trace and retrace data were observed.

In addition to RIfS measurements, *in situ* analyses of the film growth via ellipsometry in a fluidic chamber were performed. By this means, it was possible to dynamically construct PEM in flow and detect the film thickness online. The ellipsometric angles Δ and Ψ were recorded as a function of the coating time for 15 coating cycles [Fig. 4(a)]. Upon the injection of a PE, both Δ and Ψ show a stepwise decrease or increase, respectively. The film thickness calculated from the measured ellipsometric angles also shows a stepwise increase for each newly deposited layer. Furthermore, the results of the fluidic measurements correlate well with data obtained for PEM films constructed with the conventional method of statically depositing the PE layers ["static" in Fig. 4(b)]. For the statically built PEM films, three points per sample with three regions of interest per point were analyzed. Data are represented as mean ± standard deviation. Imaging ellipsometry was performed after patterning the constructed film by means of photoablation. For this purpose, the substrate was covered with a TEM grid (Plano, Wetzlar, Germany) and irradiated with 172 nm for 30 min. Imaging ellipsometry reveals a rather smooth PEM film with a thickness perfectly in accordance with the recorded data for a dynamic PE deposition in the fluidic cell [Fig. 4(c)].

In contrast to the $(PLL\text{-}PGA)_i$ model polyelectrolyte system (displaying a stepwise growth regime), an unusual adsorption kinetic was observed when the heavily phosphorylated egg yolk protein PV was utilized as the polyanion for PEM film construction [Figs. 2(b) and 5(a)]. After a few cycles of a regular, stepwise increases in optical film thickness, the deposition kinetics change drastically. The injection of a third PV layer results in an initial increase of the optical thickness in a nonlinear fashion instantly followed by a tremendous decrease in optical film thickness. It should be mentioned that this observation, referred to as overshoot (or overshooting) phenomenon was first described by Kovacevic *et al.* in 2002.[11,29] Remarkably, the optical film thickness even decreases below the level of the PLL terminated precursor film. Noteworthy, although the PEM film is solubilized to different degrees, charge reversal at the surfaces (upon the adsorption of the polyanion PV) still occurs, as indicated by the consecutive binding of the alternate PE (PLL in this case) indicating that the underlying PV is not completely desorbed. Interestingly, different salt and PE concentrations result in fundamentally different adsorption pro-

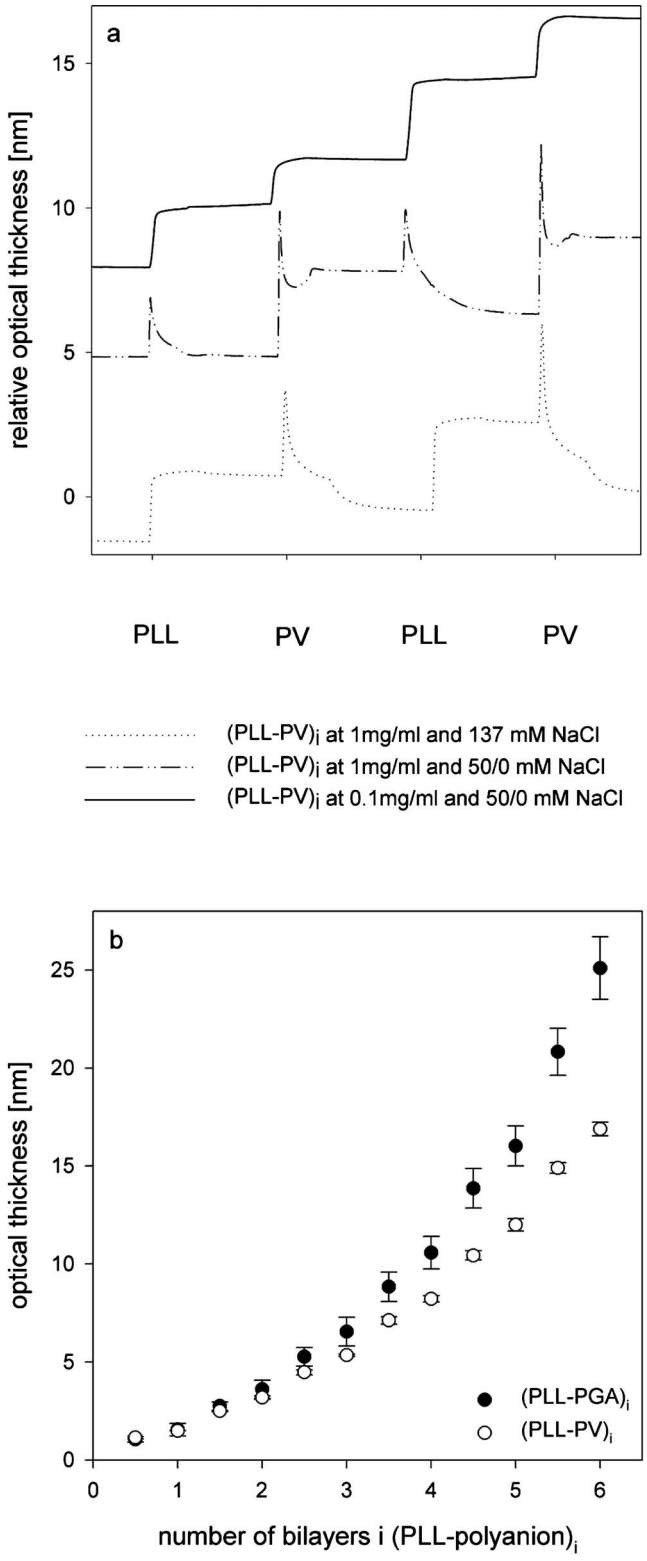

FIG. 5. (a) Comparison of different growth regimes depicted as the change in relative optical thickness (n^*d) upon the sequential addition of two double layers of PLL and PV deposited from different solutions. The dotted line (PLL and PV both 1 mg/ml and 137 mM NaCl) and the dashed line (both 1 mg/ml, PLL in 50 mM NaCl and PV without NaCl) show different degrees of overshooting while depositing either PV or both PE, respectively. The solid line (0.1 mg/ml PLL in 50 mM NaCl and 0.1 mg/ml PV without NaCl) shows a typical stepwise increase in layer thickness upon the deposition of the polyelectrolytes. (b) Comparison of growth regimes for different PE systems.

cesses as judged by the amount of overshooting observed [Fig. 5(a)]. Kovacevic *et al.*[11,29] emphasized a strong correlation of the phase behavior of PEM and PECs in solution. Both the stability of PEM and PEC in solution is strongly dependent on the concentration of low molecular weight ions and the ratio of polycations to polyanions (expressed as the mole fraction of polycations f^+). According to the bell shaped phase diagram proposed by Kovacevic *et al.*, PEMs and PECs display a glassy state for low salt concentrations [I in Fig. 6(a)]. When raising the salt concentration in the system, a phase transformation from this glassy state into a liquid state occurs [II in Fig. 6(a)]. PEM film erosion and PEC disassembly are observed when the salt concentration is further increased above a critical concentration. This PEM erosion or PEC disassembly is explained by the formation of water soluble PECs (WPECs). WPECs are formed when PE chains that initially were tethered within the PEM (or PEC) are detached and complexed by counterions (PE of opposite charge) in solution. If PE chain exchange is observed for the investigated PE systems, the large excess of either the polycation or the polyanion in solution leads to the colloidal stabilization of positively and negatively charged WPECs in solution, respectively. The formation of WPECs is observed to be more favorable when PEMs are constructed from polyanions exposing carboxylates or phosphates and polycations with tertiary or quarternary amines, as is the case for all natural proteins.[12] The major driving force is believed to be the tremendous gain in entropy due to the large degree of disorder of WPECs compared to PEM films and the greater mobility of the PE chains in WPECs. Higher salt concentrations cause an increased shielding of electrostatic interactions within the PEM and thus facilitate PEM to WPEC chain exchange. However, in 2006, Sukhishvili *et al.*[12] presented data indicating that the phase diagram for the system composed of poly(acrylic acid), quaternized poly(N-ethyl-4-vinylpyridinium bromide), and sodium chloride displays a fan shaped character [Fig. 6(b)]. According to this phase diagram, lowering the salt concentration may lead to an erosion of PEM instead of resulting in a stable liquid or glassy state. Furthermore, this model suggests that the critical salt concentration that results in PEM/PEC disassembly by means of charge shielding is independent of the mole fraction f^+. Based on their results for other PEs, Sukhishvili *et al.* proposed that a fan shaped phase diagram may be valid for most of the PE systems. However, the exact shape of its respective phase diagram remains to be elucidated for a specific polyelectrolyte system of interest.

Film buildup was monitored with RIfS in order to evaluate the influence of the salt (NaCl) and PE concentration on the PE adsorption. For a PE deposition from solutions containing 137 mM NaCl (1 mg/ml of each PE), the injection of PV causes an overshooting effect indicating that PEM erosion upon incubation with PV occurs [dotted line in Fig. 5(a)]. As shown in Fig. 5(a) (dashed line), lowering the salt concentration of the coating solution to 50 mM does not shift the system back into the vitrified state as the model of Kovacevic suggests.[11] On the contrary, injecting a PLL solution

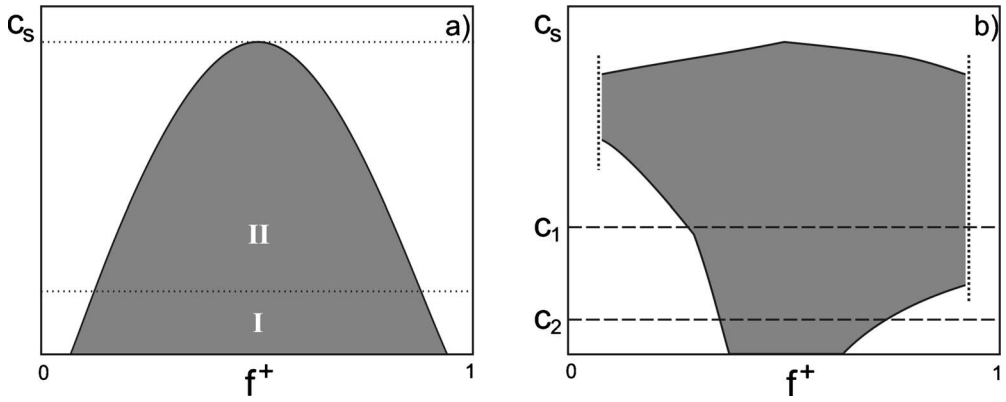

FIG. 6. Phase diagrams for PEM and PEC systems according to (a) Kovacevic (Ref. 11) and (b) Sukhishvili (Ref. 12). Stability of PEM/PEC is schematically depicted with respect to the salt concentration c_s and the mole fraction of polycations f^+ in the coating solution. Gray areas correlate to conditions where PEM/PEC are stable and white areas indicate WPEC formation and thus PEM/PEC erosion. (I) PEM/PEC in glassy state, (II) PEM/PEC in liquid state, (c_1) salt concentration 1, and (c_2) salt concentration 2.

with only 50 mM NaCl results in a destabilization and dissolution of the PEM film for both PE. This finding is in good correlation to the fan shaped phase diagrams proposed by Sukhishvili and coworkers[12] [Fig. 6(b)]. The schematic phase diagram of Sukhisvili displays film erosion for the incubation with the polyanion (corresponds to a low f^+) and PEC/PEM stability and correspondingly film growth for the deposition of the polycation (corresponds to a high f^+) for a salt concentration c1 [Fig. 6(b)]. A lower salt concentration of c2 will shift the system into an unstable state for the injection of both polyelectrolytes. However, decreasing the concentration of both polyelectrolytes to 0.1 mg/ml reconstitutes the regular, stepwise PEM growth regime [solid line, Fig. 5(a)]. From Fig. 5(b), it is obvious that both PE systems investigated display a regular PEM film buildup with the PLL-PGA system showing a more pronounced increase in growth rate.

To further support the hypothesis that the salt concentration significantly affects film stability, turbidity measurements were performed. As described earlier, there is a strong correlation between PEM and PEC stabilities. Thus, in order to investigate PEM stability, the formation of insoluble PECs, i.e., the turbidity of the samples, may be assessed. Due to the polydispersity of PLL and PV, the mass fraction R^+ of the PLL solution was adjusted instead of the mole fraction f^+ of the polycation (easily transformed with the ration of the molecular weights of the PE). High R^+ values correspond to the deposition of PLL since the concentration of polycations in solution is tremendously higher than the concentration of polyanions in the PEM film. Vice versa, the deposition of PV yields in a low R^+ value.

The highest relative absorbance was recorded for mass ratios of ~0.5 for all conditions investigated. A steep decrease in turbidity, correlated with reduced PEC/PEM stability, was observed for high and low R^+ values. This reduced stability was more pronounced for low R^+, correlating to the deposition of the polyanion PV. This result is in good accordance with the overshooting monitored for the injection of PV by means of RIfS. Lowering the salt concentration from 137 to 50 mM obviously reduces PEC formation at high R^+ (Fig. 7, left panel, circles versus triangles, respectively). The reduced PEC/PEM stability for the polycation deposition perfectly correlates with the overshooting observed after PLL injection in Fig. 5(a). Raising the NaCl concentration to 200 mM completely inhibits PEC/PEM formation (data not shown). Thus, the critical NaCl concentration (c_c) for stable PLL-PV assemblies is 137 mM $< c_c <$ 200 mM. In summary, our results on the effect of the NaCl concentration on PLL-PV PEM assembly clearly support the fan shaped phase diagram suggested by Sukhishvili.[12]

The effect of the PE concentration is not as obvious from the turbidity as from the RIfS measurements. Only marginal increases in relative absorbance upon the decrease in PE concentration from 1 to 0.1 mg/ml were observed (Fig. 7, right panel, filled versus empty circles, respectively; difference is not significant). Theoretically, the contribution of the polyanions from the film to the R^+ (or f^+ value) increases as the concentration of polycations in solution is decreased (and vice versa). Thus, for lower PE concentrations, the R^+ (or f^+) values shift to lower and higher values upon the incubation with the polycation and polyanion, respectively. However, the increments of this shift are expected to be small. The influence of the PE concentration on the buildup process detected with RIfS could be explained by stabilizing effects. A stabilization that may be imposed by the material surface SiO_2 is of course not detectable with the turbidity measurements. Nevertheless, the analyses of PEC stability by means of turbidity measurements is a valuable screening tool in order to find environmental conditions that favor stable PEM assembly. However, technologies that allow for an online monitoring of PEM film growth on substrate surfaces with a high precision and temporal resolution are of pivotal importance in (bio)material research. The RIfS detection was proven to be a valuable tool due to its accuracy (<0.01 nm optical thickness according to the manufacturer) and temporal resolution of 1 s as compared to online ellipsometry in flow-through cuvettes (~9 s). In contrast to other online monitoring techniques such as ellipsometry and QCM-D, a

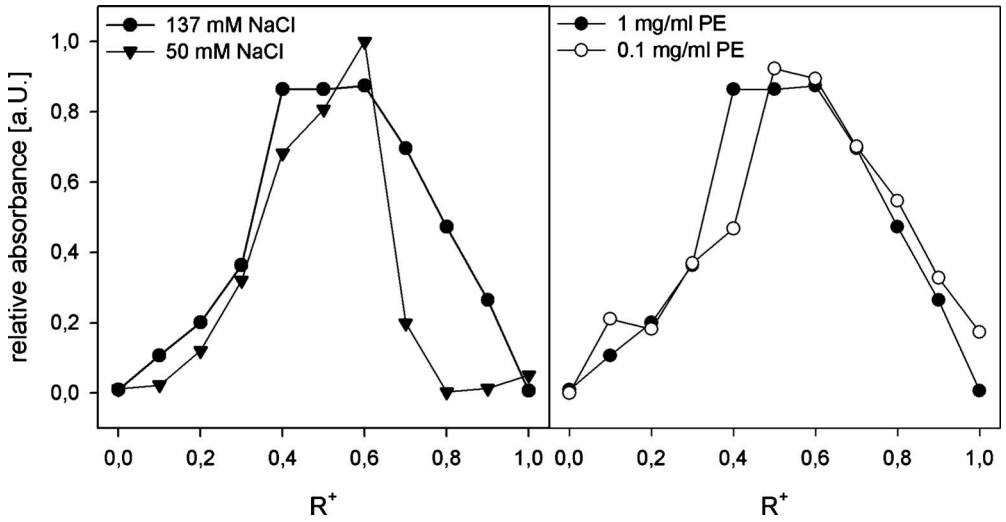

FIG. 7. Turbidity measurements of PLL/PV/NaCl mixtures supported by a Hepes buffer at *p*H 7.4. In the left panel higher (circles) and lower (triangles), salt concentrations were compared for PE concentrations of 1 mg/ml. The right panel compares the PEC formation at 137 mM NaCl from concentrated (filled circles) and diluted (empty circles) PE solutions. R^+ corresponds to the mass fraction of the respective PLL solution. Data are presented as the mean of at least three independent experiments (standard deviations range between 5% and 15%).

complex data processing (model analysis, overtone-dependency) is not required for the transformation of the measured data into film thicknesses, except for the refractive index. Although the performance is comparable to the SPR measurement setup, the RIfS technology can be performed on a sensor surface exposing SiO_2 (avoiding the need for a pretreatment of the gold surface of SPR sensors). Last but not least, both the RIfS system and the RIfS sensors are cost-effective alternatives compared to their SPR counterparts.

IV. CONCLUSIONS

The assembly of PEM films containing the biologically active molecule phosvitin is characterized by an instable growth regime. Applying RIfS detection, we were able to monitor the so-called overshooting in the range of 1–4 s with a subsequent phase of film erosion. The salt concentration of the coating solution critically influences the film stability for the deposition of PLL. While stable films are observed at a higher NaCl concentration, an overshooting was observed for lower concentrations. On the other hand, the overshooting upon PV injection was independent of the salt content in the coating solution. The data recorded with RIfS correlate well with turbidity measurements performed on polyelectrolyte complexes in solution and support the hypothesis of a fan shaped phase diagram for the PLL-PV system. When the PE (PLL and PV) concentration is lowered to 0.1 mg/ml, the system can be reverted to a regular stepwise increase in film thickness with a nonlinear growth regime. Since the sequential destabilization and solubilization (overshooting) of the multilayer are avoided, less material is needed in order to prepare coatings of a well defined quality. RIfS was found to be a valuable technology for investigating PEM film formation. In order to identify ideal coating conditions, a combination of turbidity measurements as a fast screening tool and RIfS measurements for the detailed characterization of buildup kinetics and film thicknesses can be recommended. The stability of bioactive molecules incorporated into PEM coatings in this way will certainly improve the biomaterial properties. The *in vitro* mineralization capacity of $(PLL\text{-}PV)_i$ films, constructed employing the optimized coating conditions, is under current investigation in our laboratory.

ACKNOWLEDGMENTS

The authors thank both Ms. Nadja Ehrhardt for help with ellipsometry measurements and Mr. Florian Phillip for technical assistance. Furthermore, the Deutsche Forschungsgemeinschaft (DFG) and the German Israeli Foundation (GIF) are gratefully acknowledged for their financial support.

[1]G. Decher, Science **277**, 1232 (1997).
[2]C. Picart, Curr. Med. Chem. **15**, 685 (2008).
[3]Z. Y. Tang, Y. Wang, P. Podsiadlo, and N. A. Kotov, Adv. Mater. (Weinheim, Ger.) **18**, 3203 (2006).
[4]T. Boudou, T. Crouzier, K. Ren, G. Blin, and C. Picart, Adv. Mater. (Weinheim, Ger.) **22**, 441 (2010).
[5]P. Bar-Yosef Ofir, R. Govrin-Lippman, N. Garti, and H. Furedi-Milhofer, Cryst. Growth Des. **4**, 177 (2004).
[6]M. D. Sikiric, C. Gergely, R. Elkaim, E. Wachtel, F. J. Cuisinier, and H. Furedi-Milhofer, J. Biomed. Mater. Res. Part A **89**, 759 (2008).
[7]R. N. Finn, Biol. Reprod. **76**, 926 (2007).
[8]H. Furedi-Milhofer, J. Moradian-Oldak, S. Weiner, A. Veis, K. P. Mintz, and L. Addadi, Connect. Tissue Res. **30**, 251 (1994).
[9]M. P. Richards, Poult. Sci. **76**, 152 (1997).
[10]K. Hempel, R. Rosen, D. Becher, K. Buttner, M. Hecker, and E. Z. Ron, Anal. Biochem. **385**, 208 (2009).
[11]D. Kovacevic, S. Van der Burgh, A. De Keizer, and M. A. C. Stuart, Langmuir **18**, 5607 (2002).
[12]S. A. Sukhishvili, E. Kharlampieva, and V. Izumrudov, Macromolecules **39**, 8873 (2006).
[13]J. Chluba, J. C. Voegel, G. Decher, P. Erbacher, P. Schaaf, and J. Ogier, Biomacromolecules **2**, 800 (2001).
[14]N. Jessel, F. Atalar, P. Lavalle, J. Mutterer, G. Decher, P. Schaaf, J. C. Voegel, and J. Ogier, Adv. Mater. (Weinheim, Ger.) **15**, 692 (2003).
[15]H. Zhu, J. Ji, and J. Shen, J. Biomater. Sci., Polym. Ed. **16**, 761 (2005).

[16]F. Boulmedais, B. Frisch, O. Etienne, P. Lavalle, C. Picart, J. Ogier, J. C. Voegel, P. Schaaf, and C. Egles, Biomaterials **25**, 2003 (2004).
[17]T. J. Halthur and U. M. Elofsson, Langmuir **20**, 1739 (2004).
[18]C. Porcel, P. Lavalle, V. Ball, G. Decher, B. Senger, J. C. Voegel, and P. Schaaf, Langmuir **22**, 4376 (2006).
[19]S. Y. Yang, J. D. Mendelsohn, and M. F. Rubner, Biomacromolecules **4**, 987 (2003).
[20]K. Itoh, S. Tokumi, T. Kimura, and A. Nagase, Langmuir **24**, 13426 (2008).
[21]C. Picart, R. Elkaim, L. Richert, F. Audoin, Y. Arntz, M. Da Silva Cardoso, P. Schaaf, J. C. Voegel, and B. Frisch, Adv. Funct. Mater. **15**, 83 (2005).
[22]C. Hänel and G. Gauglitz, Anal. Bioanal. Chem. **372**, 91 (2002).
[23]P. Lavalle, V. Vivet, N. Jessel, G. Decher, J. C. Voegel, P. J. Mesini, and P. Schaaf, Macromolecules **37**, 1159 (2004).
[24]F. Boulmedais, V. Ball, P. Schwinte, B. Frisch, P. Schaaf, and J. C. Voegel, Langmuir **19**, 440 (2003).
[25]N. Hoda and R. G. Larson, J. Phys. Chem. B **113**, 4232 (2009).
[26]L. Richert, P. Lavalle, D. Vautier, B. Senger, J. F. Stoltz, P. Schaaf, J. C. Voegel, and C. Picart, Biomacromolecules **3**, 1170 (2002).
[27]T. Crouzier and C. Picart, Biomacromolecules **10**, 433 (2009).
[28]L. Jourdainne, S. Lecuyer, Y. Arntz, C. Picart, P. Schaaf, B. Senger, J. C. Voegel, P. Lavalle, and T. Charitat, Langmuir **24**, 7842 (2008).
[29]D. Kovačević, S. Van der Burgh, A. De Keizer, and M. A. C. Stuart, J. Phys. Chem. B **107**, 7998 (2003).